2020

STOCHASTIC INVERSION INTEGRATING SEISMIC DATA, LITHO-FACIES PHYSICAL PROPERTIES, AND MULTIPLE-POINT GEOSTATISTICS FOR RESERVOIR CHARACTERIZATION

Mohamed Mohamed
Michigan Technological University, mohmoham@mtu.edu

STOCHASTIC INVERSION INTEGRATING SEISMIC DATA, LITHO-FACIES PHYSICAL PROPERTIES, AND MULTIPLE-POINT GEOSTATISTICS FOR RESERVOIR CHARACTERIZATION

By

Mohamed M. Abuzaied

A THESIS

Submitted in partial fulfillment of the requirements for the degree of

MASTER OF SCIENCE

In Geophysics

MICHIGAN TECHNOLOGICAL UNIVERSITY

2020

This thesis has been approved in partial fulfillment of the requirements for the Degree of MASTER OF SCIENCE in Geophysics.

Department of Geological and Mining Engineering and Sciences

Thesis Co-Advisor: *Dr. Roohollah Askari*

Thesis Co-Advisor: *Dr. Snehamoy Chatterjee*

Committee Member: *Dr. Aleksey Smirnov*

Department Chair: *Dr. Aleksey Smirnov*

Table of Contents

List of Figures…….....iv

List of Tables……..vi

Preface…….....viii

Acknowledgements……..viii

Abstract……...ix

Chapter 1: Introduction……1

1.1 Inspiration and Purposes……...……1

1.2 Chapter Glimpse…..……..3

Chapter 2: Methodology……..4

2.1 Mathematical Background……...4

2.2 Proposed Inversion Approach…….....5

2.2.1 Pre-Inversion Step……...6

2.2.2 Inversion……..……10

2.2.3 Post-Inversion Step……...14

Chapter 3: Validation and Case Study……...15

3.1 Synthetic Data……..…….15

3.1.1 Inversion Approach for Training Image as a Model Itself…….....16

3.1.2 Inversion Approach for Multiple Sets of Realizations……...22

3.2 Real Data Application…….....27

3.2.1 Exploration History……..……...…….27

3.2.2 Results……..……....29

Chapter 4: Conclusions and Future Work…….39

5 Reference List……...41

List of Figures

Figure 2.1: The workflow of the proposed inversion approach……...6

Figure 2.2: A simple clastic reservoir, two-group of litho-facies were identified……...7

Figure 2.3: A vertical section of 2D training image with 3x3 reference template……...8

Figure 2.4: The WAVESIM main components to generate four realizations……....11

Figure 2.5: The inversion components of WAVESIM realization and forward modeling12

Figure 2.6: Four realizations are produced from the WAVESIM algorithm…….13

Figure 3.1: The spatial distribution of (a) geological model (training image), (b) p-wave velocity (V_p), and (c) density (ρ)……..16

Figure 3.2: Two selected wells (W1 and W2) with their litho-facies spatial arrangement conditioned to the distribution of V_p and ρ ……...17

Figure 3.3: The bivariate distribution of the elastic properties (V_p and ρ)……...18

Figure 3.4: The input seimsic section passing through W1 and W2…….....19

Figure 3.5: Iteration results of the geological model (training image)…….....20

Figure 3.6: Three soultions generated from the inversion algorithm……20

Figure 3.7: Comparisop between the input seimsic, produced synthetic seismogram, and their residual…….....21

Figure 3.8: Probability or normalized frequency maps (E-type) for the WAVESIM realizations without constraining geophysical data …….23

Figure 3.9: Comparisopn between the input seimsic, produced synthetic seismogram, and their residual……...……24

Figure 3.10: Four solutions obtained from the inversion process for multiple sets of the WAVESIM realizations ……25

Figure 3.11: Probability or normalized frequency (E-type) and variance maps for the inversion solutions constraining geophysical data ……...26

Figure 3.12: The base map of the Penobscot offshore field……..28

Figure 3.13: A 2D structural time map of the top Middle Mississauga reservoir…… 29

Figure 3.14: Generalized stratigraphic column of the Nova-Scotia Basin 30

Figure 3.15: A structural correlation of L-30 and B-41 wells in the Penobscot field…....31

Figure 3.16: A 2D training image extracted from the 3D geological model of the Penobscot field…….....32

Figure 3.17: A 2D near-offset seismic section of the Penobscot field……...32

Figure 3.18: Two selected wells (B-41 and L-30) with their litho-facies spatial arrangement conditioned to the distribution of V_p and ρ …….....33

Figure 3.19: The bivariate distribution of the elastic properties (V_p and ρ)……..34

Figure 3.20: Well to Seismic tie process for wavelet extraction from L-30 well……..35

Figure 3.21: Comparison between the input seimsic, produced synthetic semisigram, and their residual ……..…….. 36

Figure 3.22: Four solutions obtained from the inversion process for multiple sets of the WAVESIM realizations.. 37

Figure 3.23: Probability or normalized frequency (E-type) and variance maps for the inversion solutions constraining geophysical data.....38

List of Tables

Table 3.1: Summarized values of the input parameters of the validation test..……19

Table 3.2: Summarized values of the input parameters for the multiple realizations test.22

Table 3.3: Summarized values of the input parameters for the Penobscot dataset……35

Preface

This thesis presents a manuscript to be submitted for review and publication. Each coauthor's contributions include:

- Mohamed Abuzaied: data compilation, processing, analysis, and writing
- Radwin Askari: technical assistance and proofreading
- Snehamoy Chatterjee: assistance with methods, data analysis, and proofreading

Acknowledgement

First and almost, I offer my deepest gratitude to my advisors, Dr. Radwin Askari and Dr. Snehamoy Chatterjee, for their expertise, knowledge, support, kindness, guidance, understanding, patience, and their constructive feedback, added considerably to my graduate experience these past few years. I also had the privilege of attending amazing classes with them, which significantly boosted my information about computational geosciences, seismic petrophysics, geostatistics, and reflection seismology and prepared me for what I wanted to do in my research.

My honest thanks also go to my committee members, Dr. Wayne Pennington and Dr. Aleksey Smirnov, for accepting to judge my research and their diligence in examining my thesis.

My sincere thanks to the Department of Geological and Mining Engineering and Sciences at Michigan Technological University for their encouragement and help. Particularly, Carole Asiala and Brittany Buschell for supporting me through graduate school paperwork.

I want to extend my deepest gratitude to the Fulbright US Student Program and the Binational Fulbright Commission in Egypt for their fund, boost, and encouragement; particularly, Dianne Price, Shannon Conheady, Anna Neubauer, Sarah Kidder, Gordiya Khademian, Casey O'Hara, Maggie Nassif, and Asser Hany. My academic journey at MTU would not have been possible without their believes and trustfulness in my capabilities, not only when they selected me among thousands of applicants but also during the past two years.

I'm indebted to my friends Adel Asadi and Amira Bejaoui for their significant aid; without their support, this journey would not have come to an end.

And last but not least, no words are enough to thank my parents and my siblings for their unconditional, limitless support, and encouragement. I wish I could have you surrounding me during my defense; however, your inspirational words are always in my mind that make me able to accomplish my duties.

Abstract

We proposed a novel seismic inversion approach that integrates the physical properties of litho-facies, and geophysical data, within the multiple-point geostatistical frameworks to reduce the uncertainty in predictions of litho-facies spatial arrangement away from wells or control points. The litho-facies groups (rock-type) in the well locations are defined and conditioned to the distribution of elastic properties, including P-wave velocity (V_p) and facies density (ρ) in the well locations. A conceptual geological model (training image) is utilized within a wavelet-based multiple-point geostatistical simulation (WAVESIM) algorithm to generate litho-facies realizations. In our inversion algorithm, the forward model is created by implementing the bivariate Kernel density estimation technique of the litho-facies properties (V_p and ρ) that are distributed in the well locations. The inversion approach is an iterative process, where a particular number of elastic properties (V_p and ρ) for each WAVESIM realization are drawn, and then the forward model was utilized to create synthetic seismograms. For each generated set of the WAVESIM realizations, a series of synthetic seismograms are produced, and one realization is selected that provides the best-match synthetic seismogram compared to the input seismic data using cross-correlation function. Our inversion technique was successfully applied to synthetic and field datasets. The results demonstrate the efficiency of our inversion approach to characterize highly heterogeneous reservoirs.

Chapter 1: Introduction

1.1 Inspiration and Purposes

Seismic inversion has been widely used in geophysical exploration to characterize the reservoir properties such as litho-facies distribution and the corresponding physical properties (e.g., porosity, permeability, and fluid content) (Bosch et al., 2010; Grana et al., 2012; Azevedo et al., 2015). However, an accurate estimation of the reservoir properties requires addressing the challenges stemming from the subsurface heterogeneity (Grana et al., 2012; Azevedo et al., 2015; Connolly et al., 2016). To address such challenges, a variety of inverse methodologies, both deterministic and stochastic, has been developed. Within the deterministic framework, the most common techniques are the sparse-spike and model-based, which were utilized to generate a single (best) solution (Russel, 1988; Bosch et al., 2010). Nevertheless, the uncertainty in producing a singular solution is quite a challenge. On the other hand, stochastic inversion approaches retrieve the best-fit inverse model among various scenarios and reduce the uncertainty associated with the inverted reservoir properties (Scales et al., 2001; Tarantola, 2005). The stochastic inversion process selects the best match solution with the conceptual parameters to minimize the output uncertainties (Buland et al., 2003). Previously, the stochastic inverse problem solution employed a traditional statistical approach by utilizing sequential Gaussian simulation and seismic data to generate multiple realizations of the same probability (Bortoli et al., 1993; Haas et al., 1994). In reservoir characterization, the geostatistical information mainly provides predefined, consistent geological models for any inversion algorithm, which constrain the solutions to a range of practical problems (Gonzalez et al., 2007; Grana et al., 2012).

Conventionally, geostatistical mechanisms relied on two-point statistics (i.e., variogram) such as sequential indicator simulation (SISIM) to capture the subsurface geologic structures (Deutsch et al., 1992; Journel et al., 1993). This method, however, fails to simulate complex structures such as the curvilinear channels, and to capture the massive continuity of geo-bodies. These shortcomings caused misinterpretation of the reservoir

extension and poor prediction of the reservoir properties (Guardiano et al., 1993; Tran, 1994; Boisvert et al., 2007). To overcome the limitations of two-point geostatistical models, Guardiano et al. (1993) introduced a multiple-point geostatistics (MPS) approach, where statistical information are borrowed from training images representing the possible geological scenarios (Strebelle et al., 2002; Caers et al., 2003; Arpat et al., 2005). Strebelle (2002) developed a single normal equation simulation (SNESIM), a pixel-based algorithm that is based on involving multiple points at a time, rather than using two-point variogram-based statistics, by borrowing the required multiple-point statistics from training images. Because the SNESIM technique is based on a pixel-based algorithm, it suffers from some other limitations, such as difficulty generating realistic and highly connected large-scale geologic structures (Gonzalez et al., 2007; Grana et al., 2012; Tahmasebi, 2018).

The developed sequential simulation with patterns (SIMPAT) or the modified (mSIMPAT) algorithms (Arpat, 2005; Gonzalez et al., 2007) address the limitations of the conventional SNESIM algorithm by selecting best-matched training patterns with conditioning data. However, such algorithms are computationally expensive (Grana et al., 2012; Tahmasebi, 2018). Chatterjee et al. (2012) introduced a pattern-based MPS algorithm that is based on wavelet simulation (WAVESIM). The wavelet decomposition reduces the predefined dimension of patterns produced by scanning a training image, and thus yields a faster solution while providing realistic facies simulation for complex geologies.

In this study, we present a fast stochastic inversion approach that combines the physical properties of litho-facies, geophysical data, and advanced multiple-point geostatistics algorithm to render predictable reservoir models of litho-facies spatial arrangement. In our approach, first, the litho-facies groups are defined with respect to the bivariate distribution of elastic properties (i.e., V_p and ρ) in the well locations. The bivariate distribution of the V_p and ρ in the well locations is computed based on the Kernel density estimation technique. Thereafter, the WAVESIM algorithm that derives the required geological information from the training image and conditioned to well-data generates several litho-facies realizations. In the inversion, for each WAVESIM realization, several

V_p and ρ are drawn to generate forward modeling operators that are convolved by the seismic source to produce synthetic seismograms. The inversion process is repeated for different sets of WAVESIM realizations to produce different geologic scenarios for the reservoir litho-facies distribution.

The novel proposed inversion approach was successfully applied to a reconstructed synthetic reservoir (Castro et al., 2005) and a real open-source dataset from the Penobscot offshore Field, Nova-Scotia Basin, Canada (Kendell et al., 2014).

1.2 Chapter Glimpse

Chapter 1 provides an overview of the significant role of seismic inversion in incorporating the physical properties of the litho-facies, geophysical data, and multiple-point geostatistics algorithms for predicting the shape and distribution of the reservoir in a given area.

Chapter 2 presents the mathematical background and the complete methodology of the proposed inversion algorithm.

Chapter 3 describes the validation tests and field application of the proposed inversion approach

Chapter 4 discusses the overall conclusions of this study and future work.

Chapter 2: Methodology

2.1 Mathematical Background

Theoretically, a set of model realizations represents the prototypical solution of an inverse problem, in which forward modeling of the elastic properties is inverted into synthetic data that match the real data within some tolerance (Gonzalez et al., 2007; Azizian et al., 2018). Mathematically, the inverse problem can be expressed as:

$$\delta_H(\boldsymbol{h}) = D\beta_H(\boldsymbol{h})\,\beta_G(p(\boldsymbol{h})) \tag{1}$$

where $\delta_H(\boldsymbol{h})$ is the posterior probability density, D is a normalization constant, $\beta_H(\boldsymbol{h})$ is the prior probability density. The posterior and prior probability density are defined in the model space H. Besides, $\beta_G(p(\boldsymbol{h}))$ is the likelihood function, which is a measure of the match of the model ($\boldsymbol{h}$) to the data. In equation 1, model parameterization is expressed by $\boldsymbol{h}$, and $p(\boldsymbol{h})$ is the forward-modeling operator that maps the model space into the data space (González et al., 2007, Azizian et al., 2018).

The model parameters are dissected into two subspaces: $\boldsymbol{h} = (\boldsymbol{h_g}, \boldsymbol{h_e})$ where $\boldsymbol{h_g}$ refers to the parameters of the reservoir properties such as facies, and fluid contents. At the same time, for acoustic inversion, $\boldsymbol{h_e}$ represents the elastic properties such as P-wave velocity (V_p) and density (ρ) (González et al., 2007; Azizian et al., 2018). The joint distribution of elastic properties (V_p and ρ) indicates the prior bivariate probability density for each litho-facies in $\boldsymbol{h_g}$. Based on the chain rule of conditional probability, the multivariate distribution of ($\boldsymbol{h_g}$and $\boldsymbol{h_e}$) can be estimated using the prior probability density of litho-facies parameters $\boldsymbol{h_g}$ (i.e., $\beta_H(\boldsymbol{h_g})$) and the conditional probability of elastic properties, $\boldsymbol{h_e}$, given litho-facies parameters, and can be written as:

$$\beta_H(\boldsymbol{h_g}, \boldsymbol{h_e}) = \beta_H(\boldsymbol{h_e}|\boldsymbol{h_g})\,\beta_H(\boldsymbol{h_g}) \tag{2}$$

and by merging equation (1) and (2), the posterior probability density function can be written as:

$$\delta_H(\boldsymbol{h_g}, \boldsymbol{h_e}) = D\beta_H(\boldsymbol{h_e}|\boldsymbol{h_g})\,\beta_H(\boldsymbol{h_g})\,\beta_G(p(\boldsymbol{h_g}, \boldsymbol{h_e})) \quad (3)$$

Equation 3 presents the core structure of the proposed inversion algorithm, where $\beta_H(\boldsymbol{h_e}|\boldsymbol{h_g})$ is the conditional distribution of V_p and ρ to litho-facies groups of the reservoir, and $\beta_H(\boldsymbol{h_g})$ is the prior pdf of the litho-facies groups, which can be obtained by the multiple-point geostatistical technique (Gonzalez et al., 2007; Chatterjee et al., 2012).

2.2 Proposed Inversion Approach

The proposed inversion approach is based on three main components: (i) pre-inversion, (ii) inversion loop, and (iii) post-inversion, as shown in Figure 2.1. The pre-inversion step aims to create the inputs required for the inversion loop: (a) the litho-facies groups; (b) the bivariate distribution of the elastic properties (V_p and ρ) for each litho-facies; and (c) facies simulation. The bivariate distribution of the V_p and ρ in the well location is computed based on the Kernel density estimation technique (Ruggeri et al., 2013). The facies simulation is performed using the WAVESIM algorithm conditioning to the well litho-facies data, and borrowing required information from the training image (Strebelle, 2002; Gonzalez et al., 2007; Chatterjee et al., 2012).

In our inversion loop, the values of the P-wave velocity (V_p) and rock density (ρ) for every pseudo-logs (trace) generated from the WAVESIM algorithm are simulated from the estimated kernel density. The simulated values are then fed to the forward-model, which produce the synthetic seismograms. The WAVESIM realization that offers the best-match synthetic seismogram is compared to the input seismic data using a cross-correlation function in which an appropriate cut-off (α) is selected. The inversion step is iterated based on a pseudo-random path to visit all spatial locations and produce a litho-facies solution for each set of WAVESIM realizations. In the pseudo-random path, simulation is

performed trace by trace, where pixels within the trace are simulated following a random path. For the proposed stochastic inversion, different sets of WAVESIM realizations are used for generating different inversion solutions to produce different geologic scenarios for the reservoir litho-facies distribution. A post-inversion step is used to evaluate the performance of multiple equiprobable litho-facies realizations generated from the inversion process. We have generated probability or normalized frequency maps (E-type) from multiple litho-facies simulations.

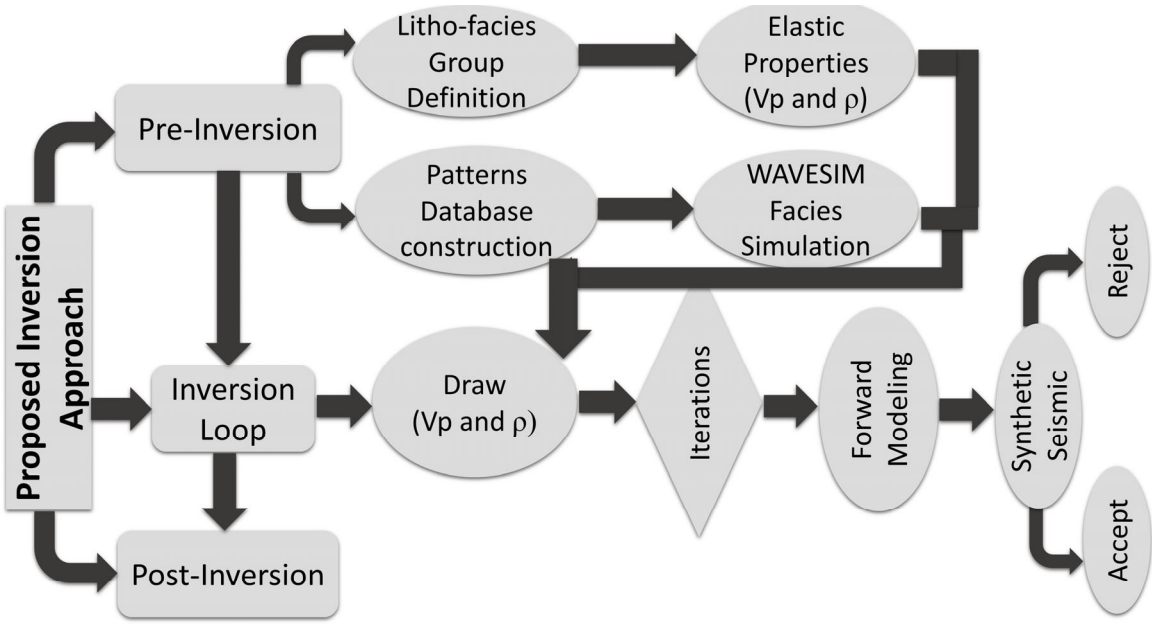

Figure 2.1**:** The workflow for the proposed inversion approach.

2.2.1 Pre-Inversion Step

As shown in Figure 2.1, the pre-inversion step includes two-differentiated procedures: litho-facies group definition, and facies simulation. Both procedures are independent and provide crucial inputs for the inversion process.

Litho-facies group definition is an essential step for seismic inversion. The term group represents the categorical variables (e.g., lithology or fluid) in the well location that has similar reservoir characteristics (Gonzalez et al., 2007; Grana et al., 2012; Azizian et al., 2018). Additionally, the bivariate distribution of the elastic properties (V_p and ρ) for each group is estimated using the elastic properties data collected from the wells, for instance, rock physics distribution conditioned to the group or $\beta_H(\boldsymbol{h_e}|\boldsymbol{h_g})$ in Equation 2. For real applications, rock physics can also be used to predict the elastic properties in the drilled wells vicinity, non-sampled areas for the proposed inversion approach (Gonzalez et al., 2007; Azizian et al., 2018).

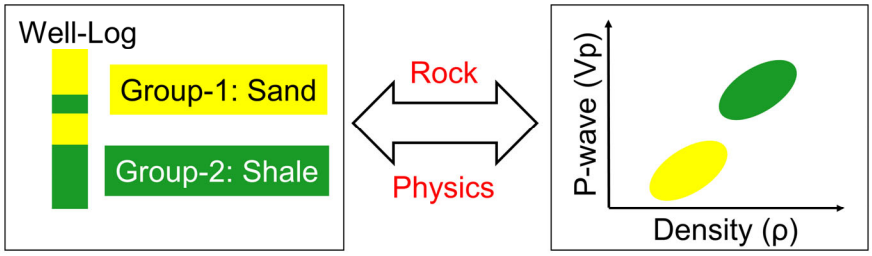

Figure 2.2: A simple clastic reservoir, two-group of litho-facies were identified, each group has as associated distribution of P-wave velocity (V_p) and density (ρ) for inverting seismic data (Gonzalez et al., 2007).

For clastic reservoirs, two simple groups (e.g., reservoir sand and barrier shale) can be identified with their V_p and ρ bivariate distributions, as shown in Figure 2.2 (Gonzalez et al., 2007). The conditional probabilities of the V_p and ρ values are calculated based on the Kernel density estimation, a non-parametric method to estimate the probability density function of a random variable using the data collected from the wells (Gonzalez et al.,

2007, Azizian et al., 2018). The estimated Kernel density estimation is then used to draw multiple V_p and ρ samples that are used for the forward modeling in the inversion loop.

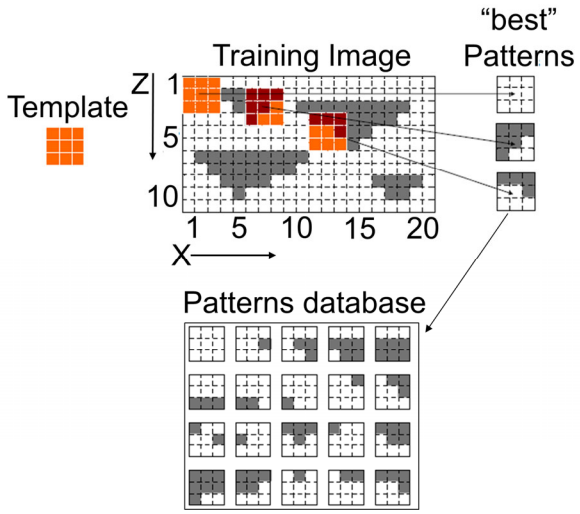

Figure 2.3: A vertical section of 2D training image with 3x3 reference template (up), a constructed pattern database (down) consists of the best selected patterns with respect to the predefined 3x3 template (Gonzalez et al., 2007).

The prior litho-facies map is the key input for the stochastic inversion model. The WAVESIM algorithm, which is a pattern-based multiple-point geostatistical simulation algorithm, is used for generating the litho-facies map. The WAVESIM algorithm, similar to other pattern-based simulation algorithms, is based on two main steps: (i) scanning a particular training image by using a predefined template with a specific size $n \times n$ to produce the pattern database; (ii) selecting the best-match pattern to the conditioning data event from the pattern database. In the following equation, $ti(e)$ defines the value of the training image (ti), where $e \in G_{(ti)}$ and $G_{(ti)}$ refer to the conventional Cartesian grid

discretizing the training image. In addition, $ti_T(e)$ designates a particular multi-point vector of $ti(e)$ inside a template (T) that is centered at the node (e) (Chatterjee et al., 2012, 2016).

$$ti_T(e) = \{ti(e + v_1), ti(e + v_2), \dots, ti(e + v_\gamma), \dots, ti(e + v_{nT})\} \quad (4)$$

where the v_γ vector defines the geometry of the n_T nodes of the template (T) and $\gamma = \{1,2, \dots, n_T\}$. The vector $v_1 = 0$ indicates the central position (e) of the template (T). Template (T) is utilized to scan the training image (ti) to generate the pattern database and store the multi-point $ti_T(e)$ vectors in the database.

Figure 2.3 shows a simple training image that is scanned by a 3x3 template to extract similar patterns from a primitive geologic channel system (Arpat, 2005; Gonzalez et al., 2007; Chatterjee et al., 2012; Grana et al., 2012). The selection of the similar pattern blocks are relied on the size of the predefined template scanned the training image. Similar patterns, consequently, are retained to construct the pattern database (Arpat, 2005). The categorical training image with N groups is converted into N sets of binary values $H_n(e), n = 1, \dots, N, e \in T$,

$$H_n(e) = \begin{cases} 1, & if\ e\ belongs\ to\ nth\ Category \\ 0, & otherwise \end{cases} \quad (5)$$

The pattern of N-categories, therefore, is presented by N sets of binary patterns where the nth binary pattern with group value 1 indicates the appearance of category n, for value 0, otherwise, indicates the nonexistence of n category in a particular position in the template (T). Figure 2.4 reveals the results of four WAVESIM realizations by visiting x-location in the well position (Gonzalez et al., 2007; Chatterjee et al., 2012).

To reduce the computational time of the pattern matching in the pattern-based simulation, instead of searching from the entire pattern database, WAVESIM only uses a limited number of representative patterns from the pattern database. To choose the representative members, similar patterns are grouped together using a clustering algorithm. The implemented WAVESIM is the most widely used clustering algorithm, i.e., k-means

clustering, where the number of clusters is selected using the gap statistics (Chatterjee and Mohanty, 2015). The representative member from each cluster is selected using the class centroid. To further reduce the computational time, the dimension reduction of the pattern database is performed using discrete wavelet transformation before applying the clustering algorithm. The wavelet decomposition reduces the dimension of patterns by preserving the significant data variability by a limited number of variables. In the simulation process, sequentially following the random path, the best-matched class is selected conditioning to the data event, and then, a random pattern is drawn from the best match class (Chatterjee et al., 2012, 2015, 2016; Mustapha et al., 2013). The similarity between the conditioning data event and the representative member of the class is measured by the Manhattan distance (Strebelle, 2002; Arpat et al., 2007; González et al., 2007; Mariethoz et al., 2010; Mariethoz et al., 2014; Chatterjee et al. 2012; Chatterjee and Dimitrakopoulos 2012). As a pre-inversion procedure, WAVESIM generates several facies realizations with the various litho-facies spatial arrangements to be used as a necessary input for the forward model in the inversion loop.

2.2.2 Inversion

The identified litho-facies groups, the bivariate distribution of V_p and ρ, the WAVESIM facies realizations, and the input seismic data are considered the main inputs for the inversion process. Through the inversion, for each litho-facies group indices in the pseudo-wells that are generated by WAVESIM, several elastic properties (V_p and ρ) are drawn using the Monte Carlo sampling. The acoustic impedance and reflection coefficients are calculated for each V_p and ρ values. These reflectivity series are convolved with the extracted wavelet from the recorded seismic data to produce a series of synthetic seismic traces (Gonzalez et al., 2007; Bosch et al., 2010; Azevedo et al., 2013). Based on the cross-correlation function with an appropriate cut-off (α: usually less than 1), the synthetic traces are compared to the input seismic traces; the best-match synthetic traces is retained. For each group of WAVESIM realizations, one realization is selected based on the cross-

correlation value that provides the best-match synthetic seismogram compared to the input seismic.

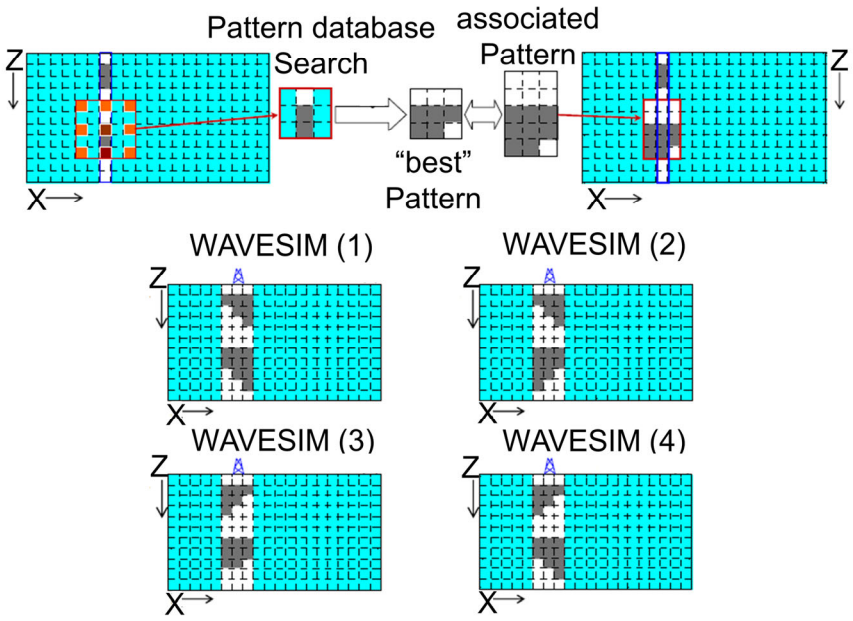

Figure 2.4: The WAVESIM main components to generate litho-facies realizations by scanning a training image that is conditioned to well-data, searching, and selecting the best-match patterns from the pattern database (González et al., 2007; Chatterjee et al., 2012).

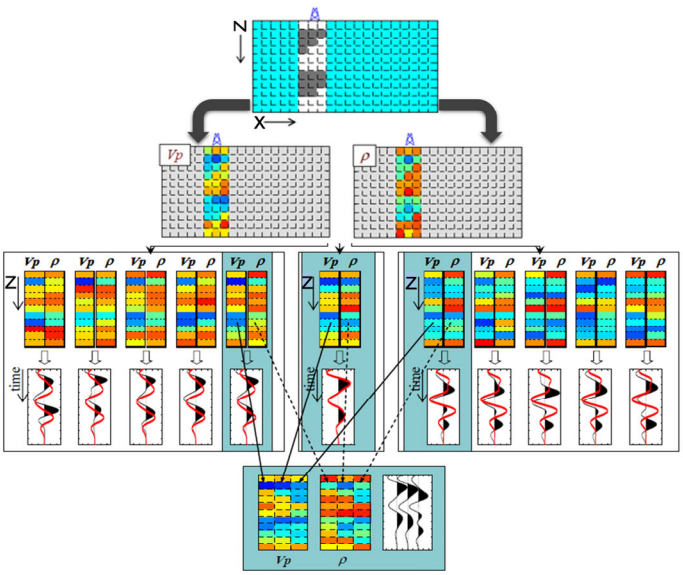

Figure 2.5: The schematic inversion components of WAVESIM simulation and forward modeling on the well position. The synthetic traces are generated through the drawing and iteration of the elastic properties. The selection process is based on the cross-correlation cut-off value of the best-match synthetic traces with the input seismic traces (V_p and ρ) (Gonzalez et al., 2007; Chatterjee et al., 2012).

For the first WAVESIM realization (Figure 2.4), since all horizontal (x) locations or common depth-point (CDP) gathers in the WAVESIM realization with the same distance from the wells, the order of visiting all surface locations (x or CDPs) is defined by a random path. Following the random path, several pseudo-wells of the elastic properties (V_p and ρ) are drawn for each group indices in the WAVESIM realization, as shown in Figure 2.5. The generated elastic properties are transformed into synthetic traces by calculating their reflection coefficient and then convolving them with the extracted wavelet from the recorded seismic data. From the deterministic wavelet extraction method using commercial software (i.e., Petrel), the wavelet can be generated by deconvolving a set of reflectivity series of a well-tied synthetic seismogram on the well location. The well to seismic tie process is based on using sonic and density logs from the available wells to generate synthetic seismogram that is well-tied with the input seismic on the well locations

(Bo et al., 2013; Azizian et al., 2018). The computed synthetic traces (black-lines), subsequently, are compared to the recorded seismic traces (red-lines) based on the cross-correlation function with a user-defined cut-off (α). The best-match synthetic traces are retained and filled with the solution grid. There might be some traces, where no pseudo-logs are accepted due to the poor cross-correlation value (less than α) between synthetic trace and the input trace. Therefore, after the first iteration of visiting all CDPs locations, some locations can still be empty. Then the subsequent iterations proceed. When it goes to a previously filled location, it only accepts pseudo-logs that give a better α value compared to the previous value.

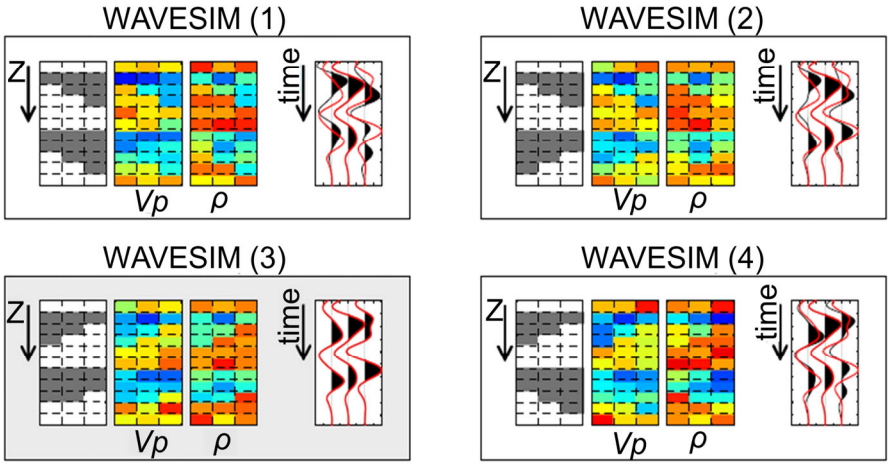

Figure 2.6: Four realizations are produced from the WAVESIM algorithm in Figure 4 and their inversion results; the red synthetic traces present the input seismic, which are compared to the generated black traces from the inversion process. WAVESIM three represents the best realization that produces the best-match synthetic traces with input seismic (Gonzalez et al., 2007, Chatterjee et al., 2012).

The proposed inversion approach is terminated when all traces are filled. Figure 2.6 shows the results of the inversion loop for the four WAVWSIM realizations. For each generated set of realizations, one realization is selected that provides the best-match synthetic seismic compared to the input seismic data. The solution grid, eventually, is filled with the accepted pseudo-logs of the V_p and ρ values for all group indices in addition to the corresponding synthetic traces.

2.2.3 Post-Inversion Step

Each best-realization that is selected from the inversion represents an equiprobable geologic scenario of the spatial arrangement of the litho-facies for a given reservoir. For generating multiple equiprobable reservoir's litho-facies maps, the inversion loop is repeated with different sets of the WAVESIM realizations to generate an optimized solution from the inversion process that preserves the major characteristics of the reservoir. The generated probability or normalized frequency map (E-type) of all realizations exhibits the maximum occurrence of each litho-facies group at each cell on the solution grid. The probability or normalized frequency map (E-type) is considered as the best visualization tool for optimized solutions (Gonzalez et al., 2007). The variance map is also generated from all realizations by the inversion process to evaluate the uncertainty of the inversion model.

Chapter 3: Validation and Case Study

The proposed inversion approach is applied to synthetic and real datasets. The synthetic dataset is generated with respect to a reconstructed synthetic reservoir, Stanford VI-E (Castro et al., 2005). The real data is from the Penobscot offshore field, Nova-Scotia Basin, Canada. The objective of the stochastic solution is to predict the shape and distribution of the geologic structures for a given reservoir. In each test, the elastic properties for every group indices are inverted using the proposed inversion process to predict the spatial arrangement of the litho-facies in the reservoir.

For the synthetic data set, two tests were performed. In the first test, the training image is used as the model itself to verify the inversion approach by forecasting the shape and distribution of the sand channels in the inverted solutions. This test validates the proposed inversion method by using the training image as the model itself to predict the shape and distribution of the reservoir channels that are generated through the inversion process. The second test examines the ability of the proposed method by providing a set of equiprobable realizations that are produced by using the WAVESIM algorithm. For the real dataset, the equiprobable realizations of geological models were developed using WAVESIM and borrowing information from the training image. The training image for the real application was prepared using the geological interpretation of the well data using expert geological knowledge.

3.1 Synthetic Data

3.1.1 Inversion Approach for Training Image as a Model Itself

Figure 3.1 shows a 2D cross-section of a simplified, two litho-facies (two groups); channel sand represents the target hydrocarbon reservoir, and the background shale is assumed impermeable. This cross-section in Figure 3.1 depicts the training image for the proposed inversion technique. The cross-section thickness is 80 m (cells) in the z-direction

and contains 150 CDPs in the x-direction with a total length of 3755 m. Also, Figure 3.1 displays the distribution of the elastic properties V_p (P-wave velocities) and ρ (densities) of the predefined cross-section (González et al., 2007).

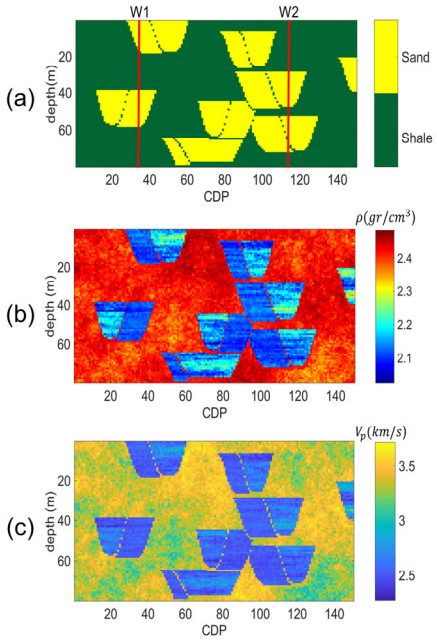

Figure 3.1: The spatial distribution of the (a) geological model (training image) includes the two selected wells (W1 at CDP 35 and W2 at CDP 115), (b) density (ρ), and (c) P-wave velocity (V_p).

Figure 3.2 shows the distribution of the elastic properties (V_p and ρ) conditioned to the spatial arrangement of the two litho-facies groups (i.e., channel sand and background shale) on the position of the selected wells (W1 and W2). The elastic properties of the channel sand and background shale are well-differentiated and computed from the mean, variance, and covariance for each group indices. Additionally, Figure 3.3 shows the bivariate distribution of the V_p and ρ values in the well locations, using the Kernel density estimation method for each litho-facies group indices (see Equations 2 and 3). The

generated cdf and pdf plots in Figure 3.3 reveals that W1 well has well-discriminated V_p and ρ for background shale and channel sand. Therefore, multiple draws of the elastic properties (V_p and ρ) from W1 well have been used in the inversion loop. The WAVESIM algorithm generates multiple litho-facies realizations by borrowing the required information from the geological model (Figure 3.1) and is conditioned to the litho-facies group information at the selected wells (W1 and W2). Subsequently, the likelihoods of V_p and ρ are drawn trace by trace at all CDP locations in the WAVESIM realizations.

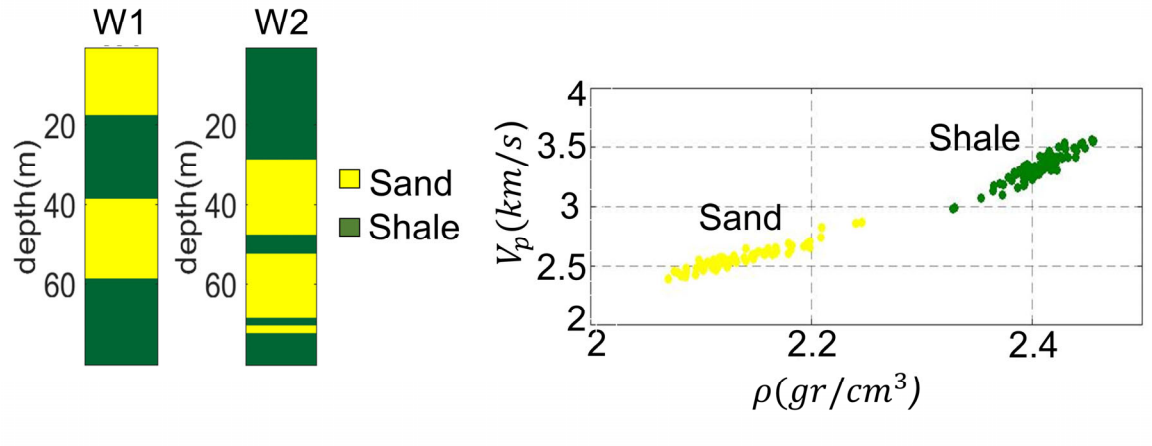

Figure 3.2: Two selected wells, W1 at CDP 35 and W2 at CDP 115, from the geological model shown in Figure 3.1. The two-group litho-facies spatial arrangement in the two wells (left) and a cross-plot of V_p and ρ values are colored by the two groups (right).

The input seismic section in the inversion process is computed by a convolution model using a standard Ricker wavelet (15 Hz - central frequency), as shown in Figure 3.4. This bandwidth is intentionally assumed to depict the value of utilizing the proposed inversion approach for such complex geologic structures (i.e., channels) that could not

directly be defined from observing seismic amplitudes (González et al., 2007). Table 3.1 shows the values of the input parameters (template size, number of draws, iteration number, number of samples, and cut-off factor) in the first test. The decision to select these values is based on trials and observations. These parameters are user-defined and varied based on the MPS algorithm, and the inversion procedure.

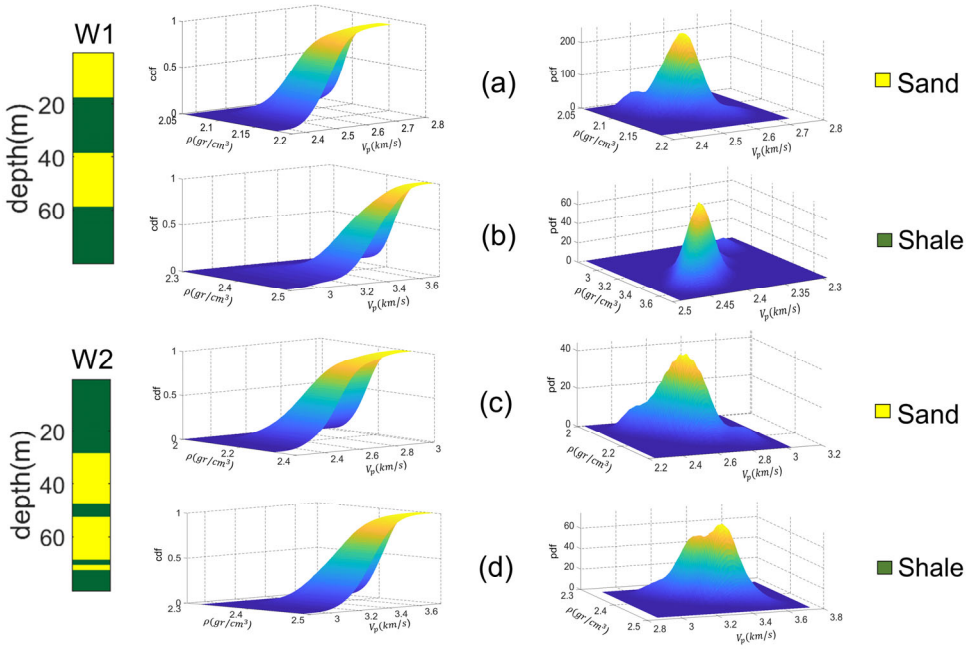

Figure 3.3: For W1 well, (a) bivariate cdf and pdf cross-plots for sand and (b) bivariate cdf and pdf cross-plots for shale. Similarly, for W2 well, (c) bivariate cdf and pdf cross-plots for sand and (d) bivariate cdf and pdf cross-plots for shale.

Table 3.1: Summarized values of the input parameters for the validation test.

Parameter description	**Value**
WAVESIM template size	(11,11)
Elastic properties draw	20
Elastic properties iterations per CDP	20
Sampled CDP	1
Cross-correlation factor (α)	0.8

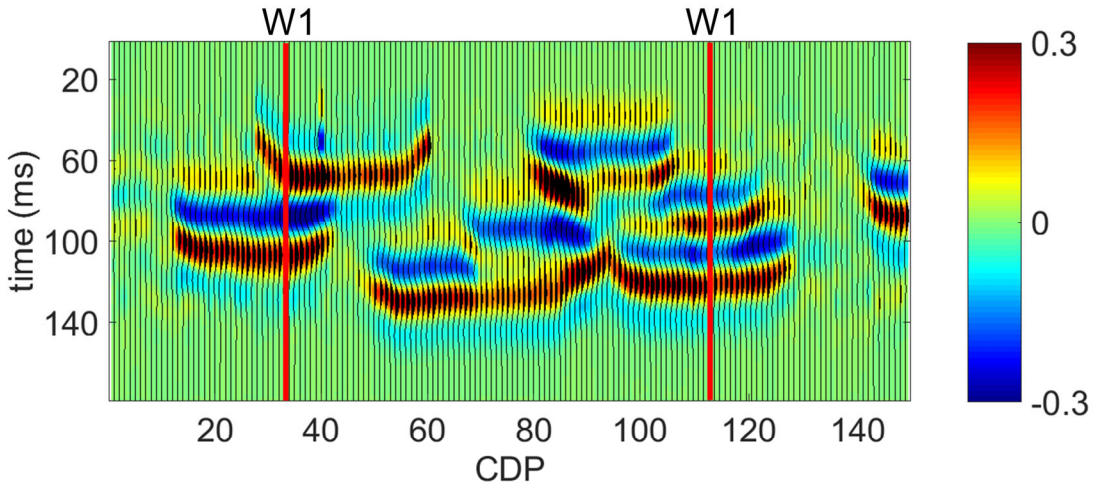

Figure 3.4: The input seismic section passing through the two selected wells in the geological model (training image) in Figure 3.1, which was estimated by utilizing a standard Ricker wavelet with 15 Hz of the central frequency, and was plotted every fourth trace with a wiggle trace.

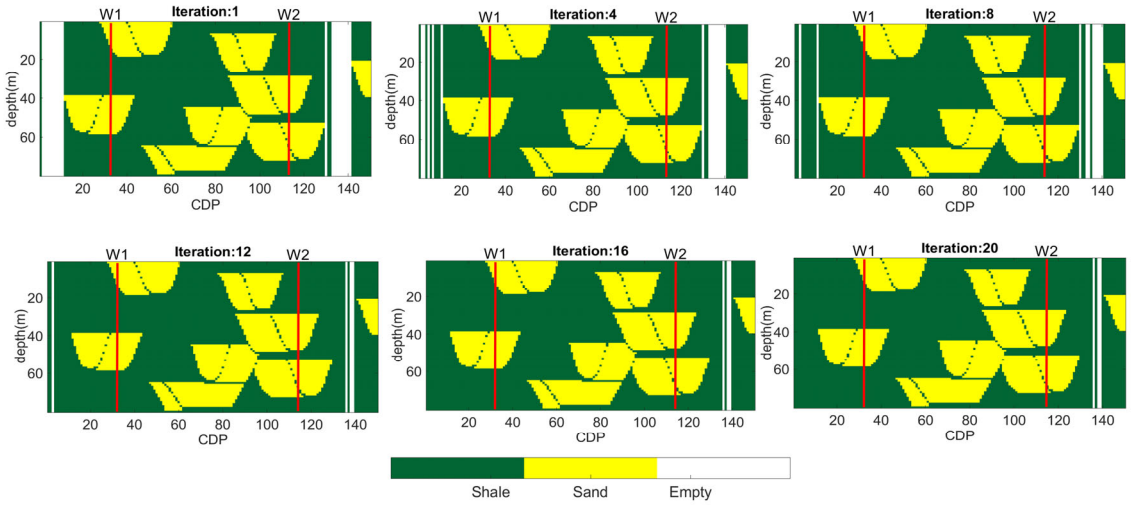

Figure 3.5: Iteration results obtained from the inversion process for the geological model (training image) in Figure 3.1 after 20 iterations and 20 draws.

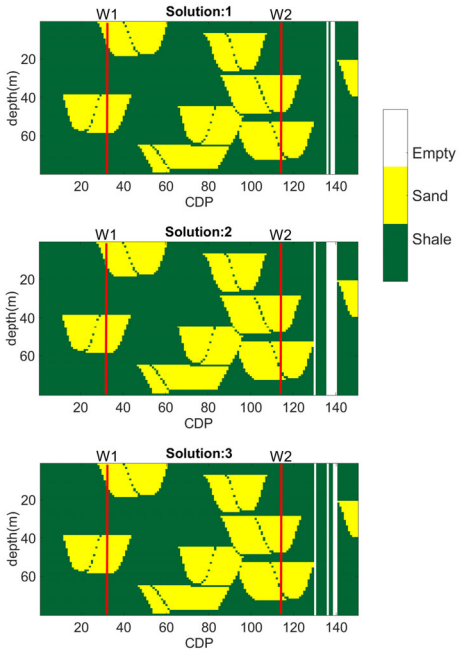

Figure 3.6: Three solutions by running the proposed inversion process with the same criterion parameters in Table 3.1 separately.

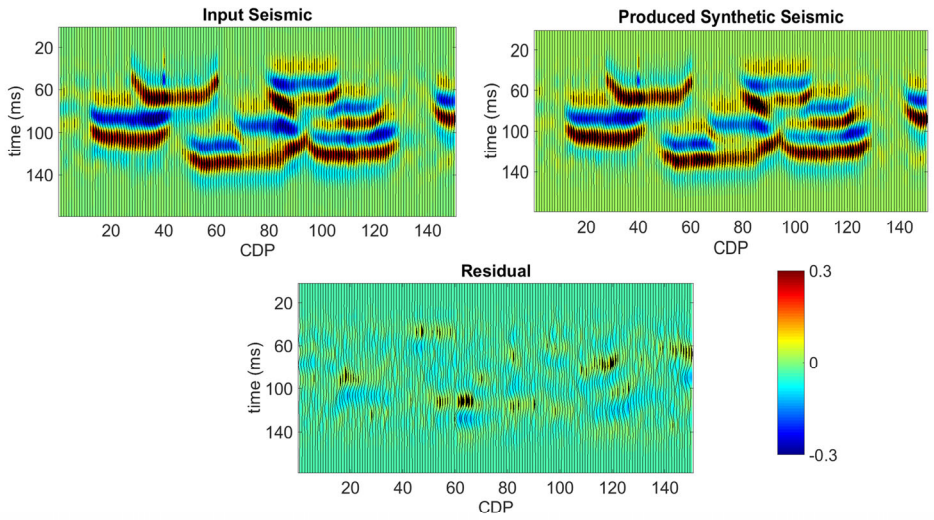

Figure 3.7: Input seismic, produced synthetic seismic, and the difference sample-by-sample between them (residual) for all solutions after 20 iterations of the proposed inversion approach.

Figure 3.5 shows several results of twenty iterations, where there is a significant enhancement in the initial model through iterations. In the initial iterations (iteration 1 and 2), substantial portions of CDPs are not filled because no pseudo-logs are accepted due to the low cross-correlation value (lower than the cut-off (α)). The empty CDPs are then getting filled with the increasing iteration number (iteration 12, 16, 20). In this synthetic test, the most difficult locations to fill were the first ten CDPs, besides the CDPs between 133 and 137, due to the presence of low acoustic impedance shale in the entire CDPs that produces low seismic amplitudes. However, by increasing the number of draws and iterations, these empty locations are started to be filled, except for a few spots of CDPs. By running the inversion several times with the same criterion parameters (Table 3.1), the resulted solutions were almost similar. Figure 3.6 shows three equiprobable final realizations from the inversion; each solution was obtained from a separate run for the proposed inversion approach with the same criterion parameters. Figure 3.7 shows the best-

match synthetic seismogram that was generated from the first solution and compared it to the input seismic data. Likewise, the other solutions in Figure 3.7 provide similar results for the generated synthetic seismograms. These solutions are quite identical and demonstrate the inversion performance in reducing the uncertainty of predicting the litho-facies spatial distribution for the reconstructed Stanford VI-E synthetic reservoir.

Table 3.2: Summarized values of the input parameters for multiple realizations.

Parameter description	**Value**
WAVESIM template size	(11,11)
Elastic properties draw	30
Elastic properties iterations per CDP	6
Sampled CDP	1
Cross-correlation factor (α)	0.8
WAVESIM realizations per CDP	10

3.1.2 Inversion Approach for Multiple Sets of Realizations

In this test, the WAVESIM algorithm was used to simulate equiprobable prior geological models from a conceptual geological model, (i.e., training image), to produce several litho-facies realizations (Gonzalez et al., 2007; Chatterjee et al., 2012). Table 3.2 shows the values for the assigned parameters that were used in the second test. Table 3.2

parameters have been selected are very similar to Table 3.1, except the number of draws and the number of repetitions due to the litho-facies distribution of the generated realizations has distinct spatial arrangement than in the conceptual geological model used in the previous test. As it has mentioned above, these values in Table 3.2 are user-defined and can be modified for various datasets accordingly. In the inversion process, each solution is generated by visiting all surface locations for each realization eight times until filling the solution grid.

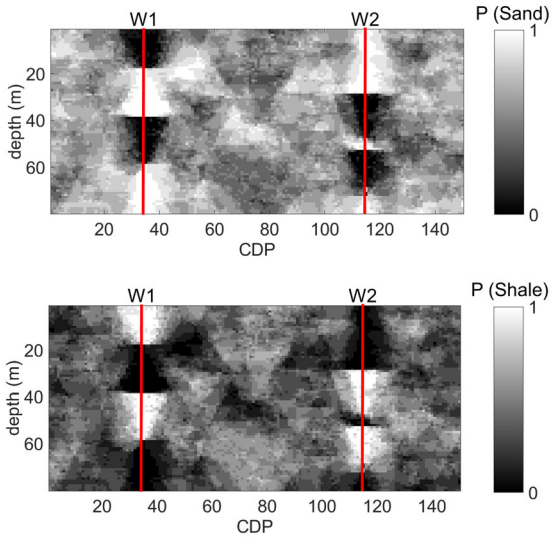

Figure 3.8: Probability or normalized frequency maps (E-type) for the two assigned lithofacies groups (sand and shale), from the geological model in Figure 3.1, are estimated with ten WAVESIM realizations without constraining seismic data, and conditioning only to the two selected wells (W1 at CDP 35 and W2 at CDP 115).

The probability or normalized frequency map (E-type) is calculated cell-by-cell by counting the number of occurrences of each group and dividing by the cumulative number of solutions. The probability of each cell concerning each group indices is a crucial element in generating the normalized frequency map, which is one of the best ways to visualize results (González et al., 2007; Bosch et al., 2010). Figure 3.8 shows E-type maps for the two litho-facies groups (channel sand and background shale), generated from ten WAVESIM realizations without constraining seismic data. It is observed from the probability maps that the higher probability values are observed near the well locations (W1 at CDP 35 and W2 at CDP 115). However, as expected, the probability values are low at the location away from the two wells. Therefore, the WAVESIM realizations cannot precisely simulate the geological features away from well locations without constraining the geophysical data.

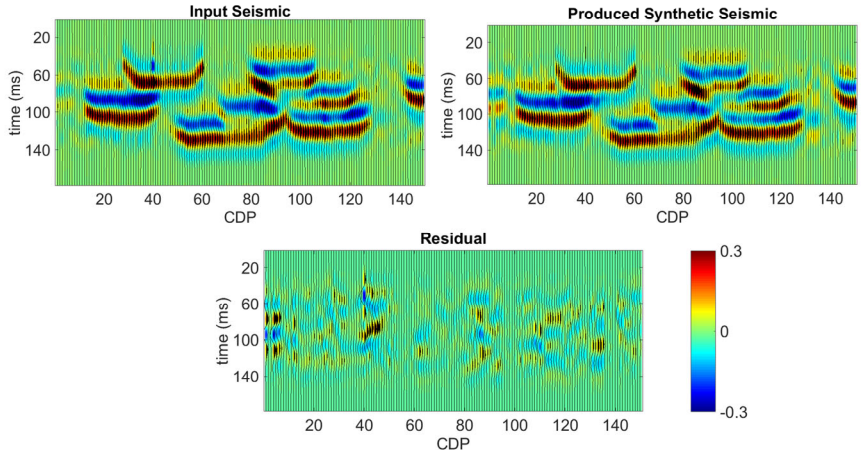

Figure 3.9: Input seismic, produced synthetic seismic, and the difference sample-by-sample between them (residual) for multiple sets of WAVESIM realizations after six iterations and 30 draws of the proposed inversion approach.

The generated synthetic seismogram after 30 draws and six iterations of the elastic properties through the inversion is compared with the recorded seismic data, as shown in Figure 3.9. For all solutions that are obtained from the inversion loop for multiple sets of WAVESIM realizations, after six iterations, the difference (sample-by-sample) between the generated synthetic seismogram and the input seismic data remains constant. The sample-by-sample values are estimated from the residual seismic section and reveal tiny differences between the original and synthetic seismograms, which lead to the borders of the channels were less continuous with gaps within some channels for some obtained solutions from the inversion loop, as shown in Figure 3.10.

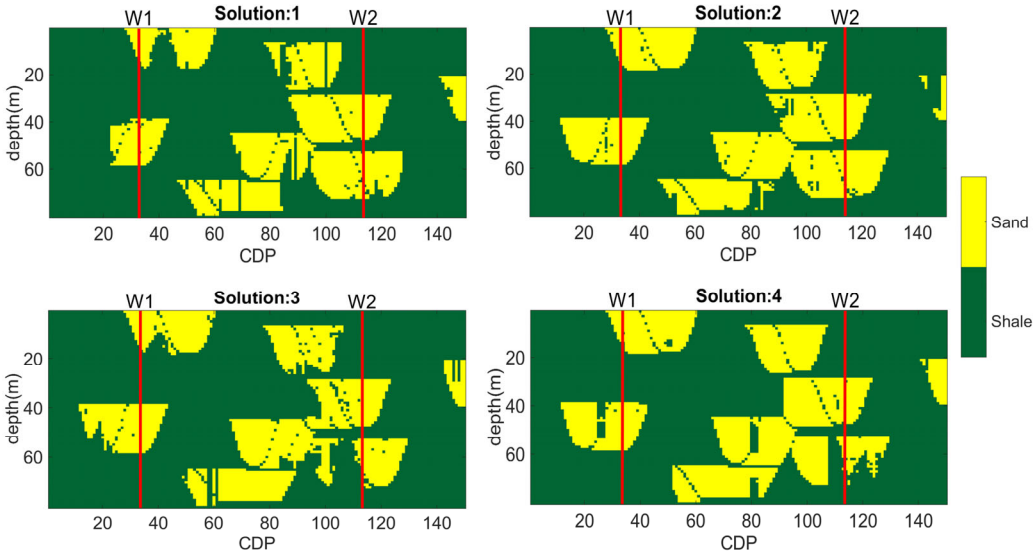

Figure 3.10**:** Four solutions obtained from multiple sets of the WAVESIM realizations after six iterations and 30 draws of the proposed inversion approach.

In the inversion, different sets of WAVESIM realizations were used as prior solutions for generating different inversion solutions to produce different geologic scenarios for the reservoir litho-facies distribution. The normalized frequency or probability (E-type) and variance maps for the channel sand and background shale are generated, and are shown in Figure 3.11. The shape and distribution of the major geologic bodies (sand channels) are precisely localized and observed in the probability maps. It was also observed from the probability maps of the inversion solutions that probability values away from the well locations are significantly improved as compared to the probability maps from WAVESIM (Figure 3.8). From the variance map, it can be seen that the variance values are very low near to the wells and increases away from the wells. Overall, the stochastic solutions have validated the efficiency of the proposed inversion approach.

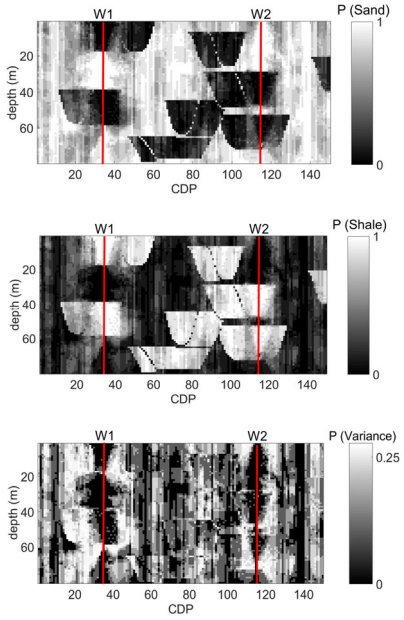

Figure 3.11: Probability or normalized frequency (E-type) and variance maps for the two assigned lithofacies groups (sand and shale), from the geological model in Figure 3.1, are estimated with multiple sets of the WAVESIM realizations constrain seismic data, which were computed after 30 draws and six iterations of the proposed inversion approach.

3.2 Real Data Application

3.2.1 Exploration History

Figure 3.12 shows the location of the Penobscot offshore field (Kendell et al., 2014). Figure 3.13 depicts a 2D time map that exhibiting the structure regime in this area, where a down-thrown fault block confines the Middle Mississauga sand reservoir. The discovered L-30 well encountered seven thin sand channel pay zones; all of them have a thickness of less than 0.6 m. This great discovery motivated the Petro-Canada-Shell to drill another exploratory well B-41 in the up-dip from the discovered L-30 well, to follow the reservoir extension in this area and evaluate the oil reserves in this field. The B-41 well was drilled around 3800 m northwest the discovered well; however, no meaningful oil and gas pay zones were estimated, and their traditional tools were failed to follow the discovered reservoir. Although the formation well tops in well B-41 is about 15 m above L-30 formation tops, the seven thin sand channels in L-30 well were evanesced in the B-41 well. The unexpected results have caused a great dilemma about future drilling activities in the Penobscot field (Kendell et al., 2014).

The stratigraphic column for the Nova-Scotia basin depicts a deltaic depositional environment; these deposits consist of sandstone, siltstone, and shale interbedded with limestone streaks, as shown in Figure 3.14 (Campbell et al., 2015). Missisauga reservoir was trapped between Upper and Lower Missisauga formation (Kendell et al., 2014). The reservoir quantitative parameters (e.g., lithology, V_P, and ρ) were obtained from the logs of wells L-30 and B-41. The 2D seismic line was extracted from a 3D seismic cube in the intersecting path between the two well locations. A 2D geologic cross-section (training image) was acquired from a 3D facies cube that was created through Petrel, in the direction parallel to the arbitrary seismic line. All the data mentioned above were used as input parameters for the proposed inversion approach. Based on the geological information in the Penobscot area obtained from the two wells; Missisauga reservoir encounters three-group of lithology (i.e., Channel sand, silty-sand, and barrier shale), the silty-sand streaks has merged with shale due to their similar properties as seal rocks in the reservoir zone.

Therefore, two groups of litho-facies were defined; channel sand and barrier shale. Figure 3.15 shows the crucial well logs from the selected wells (L-30 and B-41). Gamma-ray (GR), sonic velocity (V_p), and density (ρ) are the assigned logs that could be used in the inversion approach.

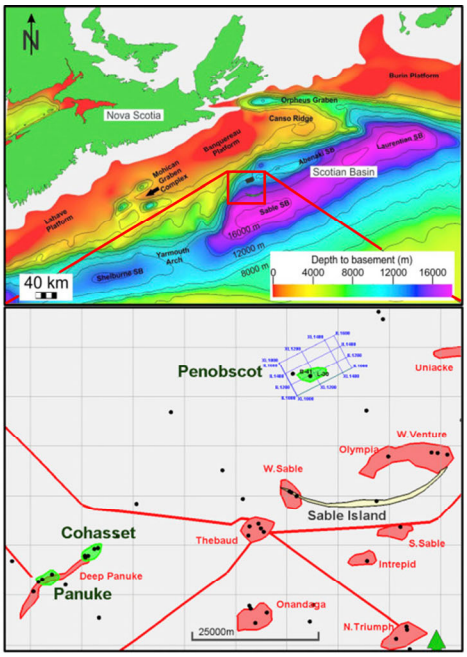

Figure 3.12: The base map of the given study area, the Penobscot offshore field, Nova-Scotia Basin, Canada (Campbell et al., 2015).

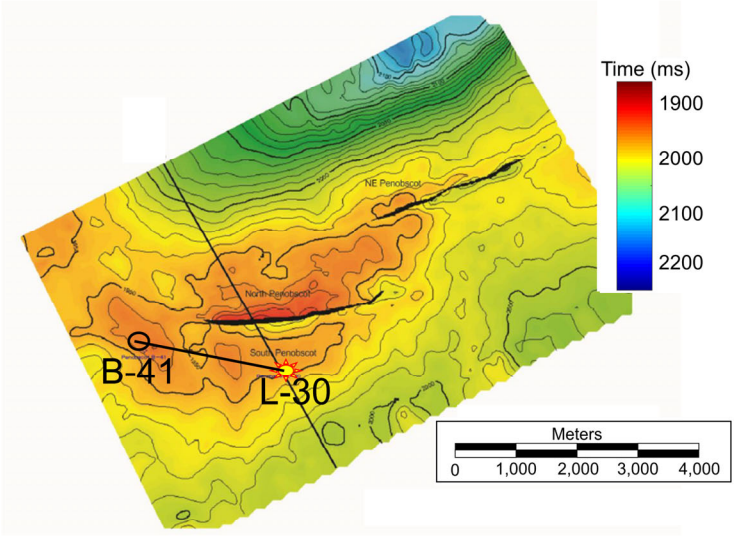

Figure 3.13: A 2D structural time map of the top Middle Mississauga reservoir encounters the two selected wells B-41 and L-30 (Kendell et al., 2014).

3.2.2 Results

Figure 3.16 shows the 2D training image that was derived from a 3D geologic model. This model represents the distribution of channel sand and barrier shale. Numerically, the 3D geologic model has confined 71 and 110 cells in the horizontal x and y directions and 20 layers in the vertical direction z. The horizontal x and y dimensions are 50x50 for each cell. In the vertical direction, 15 cells of the model are covered 150 feet of the reservoir, 10 feet for each cell. The size of the 2D training image is 152 in the x-direction and 74 in the z-direction. The input seismic section for the inversion process is extracted from the Petro-Canada shell's 3D volume and covered the distance between the selected wells (B-41 and L-30); around 3800 m of seismic traces (CDPs) are separated by a 25 m distance in between, as shown in Figure 3.17. The geologic structure interpretation in the Penobscot field is based on seismic data, and the flatten surface at 60 ms presents the target reservoir.

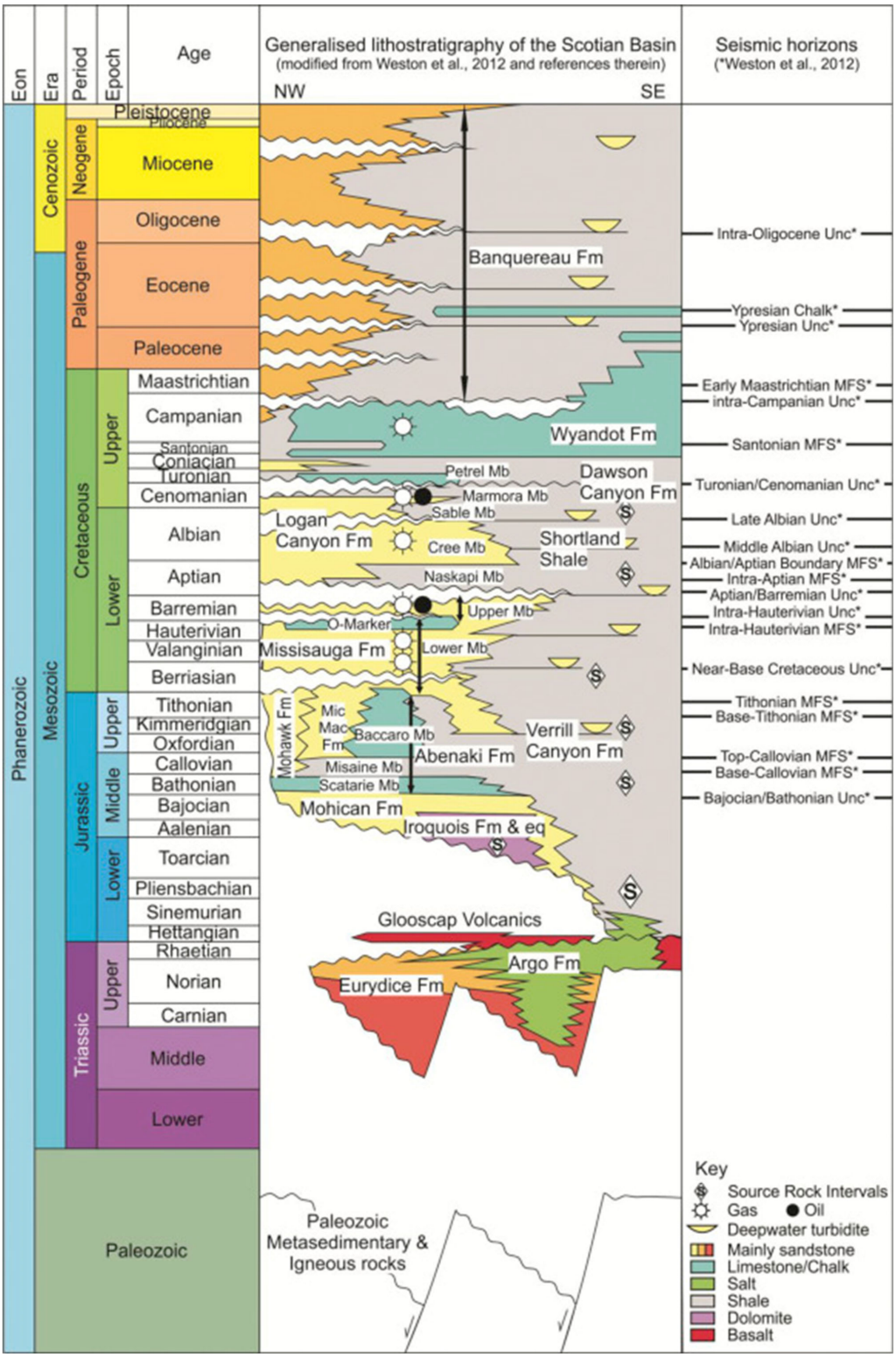

Figure 3.14: Generalized stratigraphic column of the Nova-Scotia Basin, Canada (Campbell et al., 2015).

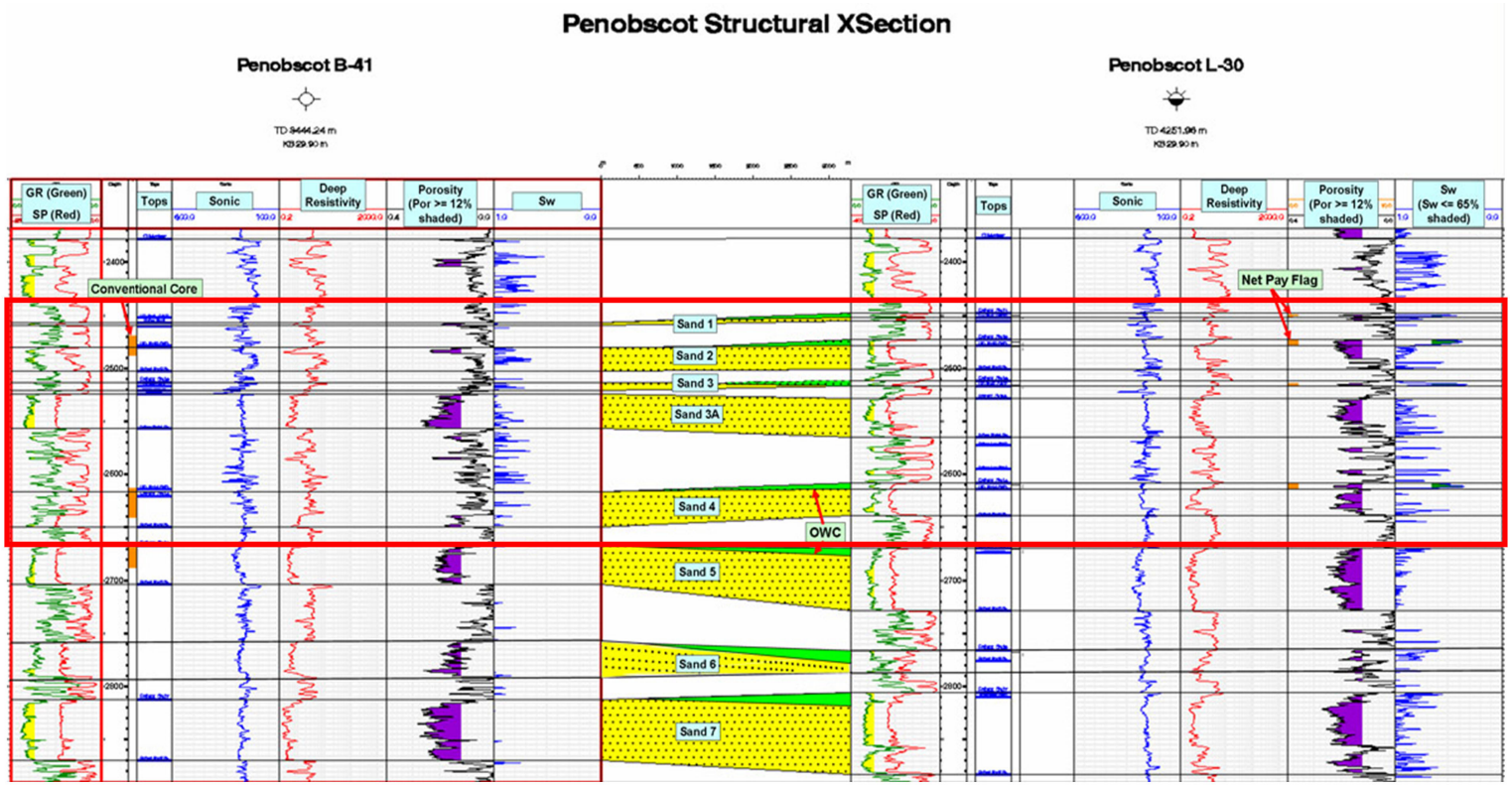

Figure 3.15: A structural correlation of the Penobscot field for the two selected wells B-41 and L-30, with the well logs data such as gamma-ray, density, and sonic. The red box represents the interested Missisauga reservoir zone. (Kendell et al., 2014).

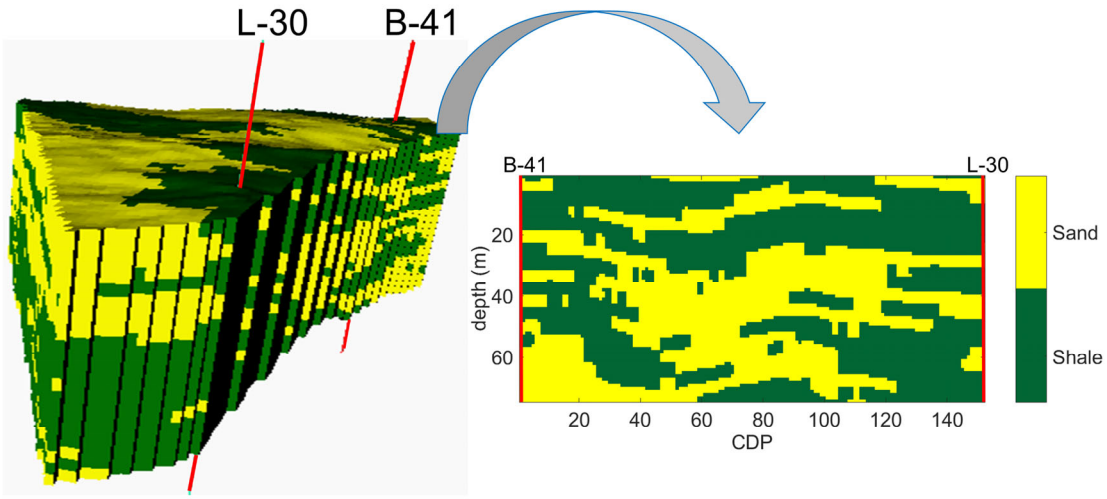

Figure 3.16: A 2D training image extracted from the 3D geological model of the Penobscot field. B-41 at CDP 1 and L-30 at CDP 152 are the two selected wells for this study area.

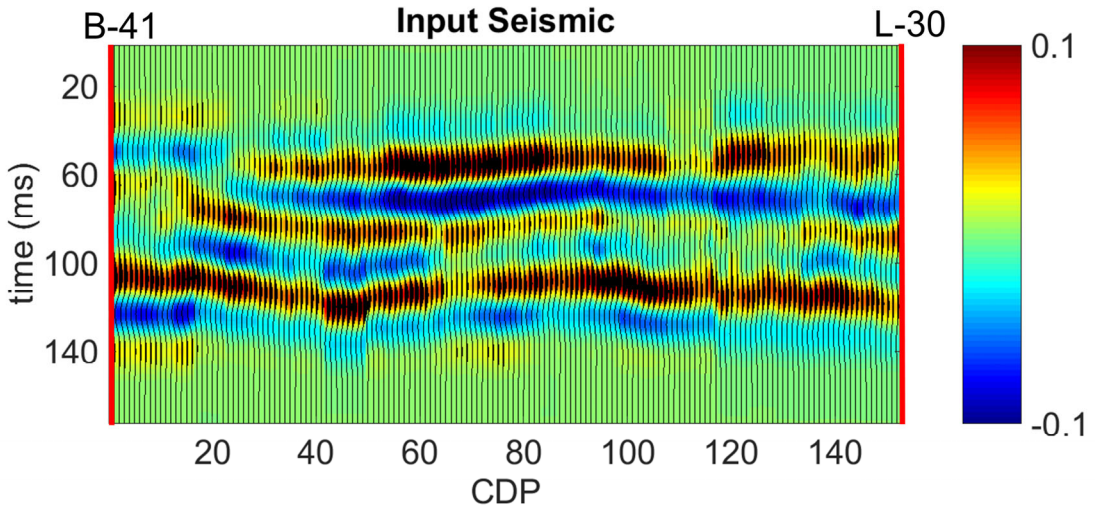

Figure 3.17: A 2D near-offset seismic data of the Penobscot field depicts the locations of the two selected wells, B-41, and L-30.

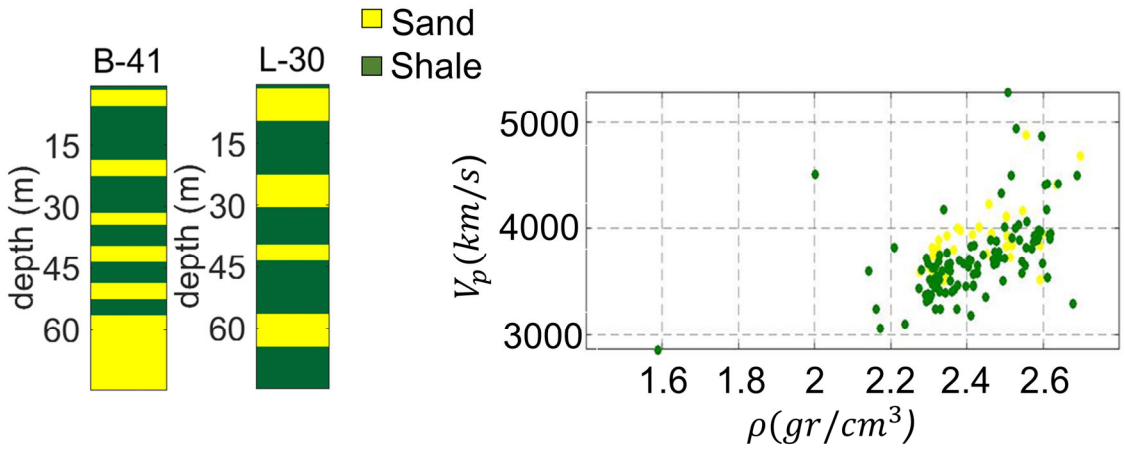

Figure 3.18: Two selected wells, B-41 at CDP 1 and L-30 at CDP 152, from the geological model shown in Figure 3.16. The two-group facies distribution alongside the two wells (left) and a plot of V_p and ρ values has colored by the two groups (right).

Figure 3.18 shows the spatial distribution of the litho-facies groups (i.e., channel sand and barrier shale) on the B-41 and L-30 wells, conditioned to the distribution of the elastic properties (V_p and ρ). The V_p and ρ of the barrier shale group have overlapped the elastic properties of the channel sand group. With increasing depth, the elastic properties of the sand group cannot be distinctly differentiated from the V_p and ρ of the shale group, as well as, the presence of the interbedded silty-sand facies with shale causes this overlap with intermediate elastic properties. Figure 3.19 unveils the bivariate distribution of the values of V_p and ρ that is estimated by the Kernel density estimation technique for the assigned litho-facies groups (Figure 3.18). The generated cdf and pdf plots in Figure 3.19 shows that L-30 well has well-discriminated V_p and ρ for background shale and channel sand than B-41 well. Consequently, multiple draws of V_p and ρ from L-30 well have been used in the inversion approach. Table 3.3 summarizes the values of the input parameters for this application. Before the inversion step, the pattern database is constructed by

scanning the training image with an 11-by-11 template through the WAVESIM algorithm. The WAVESIM technique produces ten lithofacies realizations for the inversion process. As mentioned earlier, all the assigned values of the input parameters for the inversion loop were selected after several trials and observations.

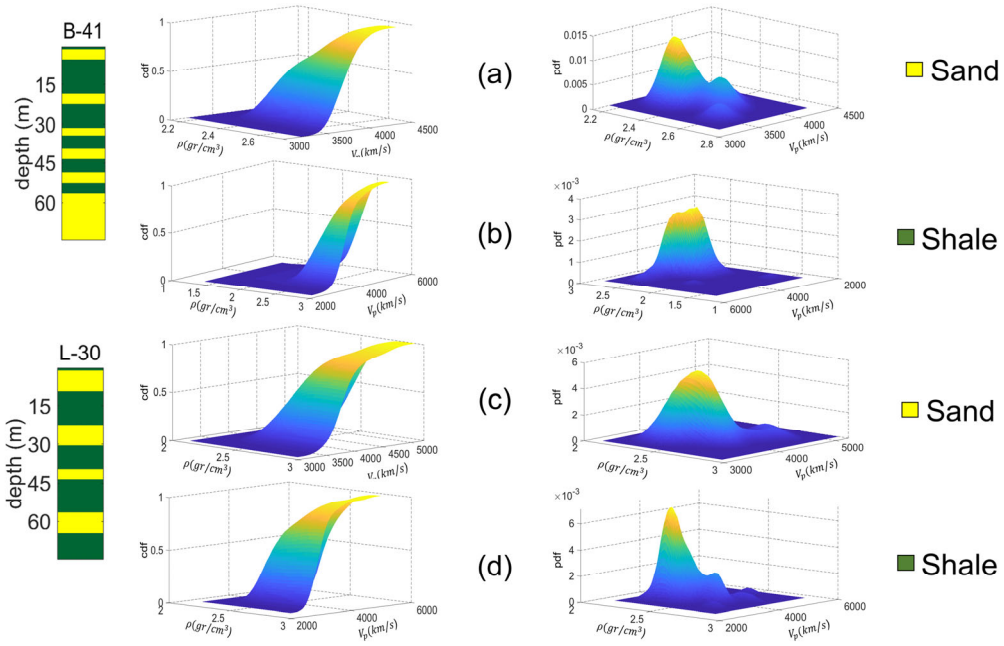

Figure 3.19: For B-41 well, (a) bivariate cdf and pdf cross-plots for sand and (b) bivariate cdf and pdf cross-plots for shale. Similarly, for L-30 well, (c) bivariate cdf and pdf cross-plots for sand and (d) bivariate cdf and pdf cross-plots for shale.

Table 3.3: Summarized values of the input parameters for the Penobscot dataset.

Parameter description	**Value**
WAVESIM template size	(11,11)
Elastic properties draw	60
Elastic properties iterations per CDP	8
Sampled CDP	1
Cross-correlation factor (α)	0.7
WAVESIM realizations per CDP	10

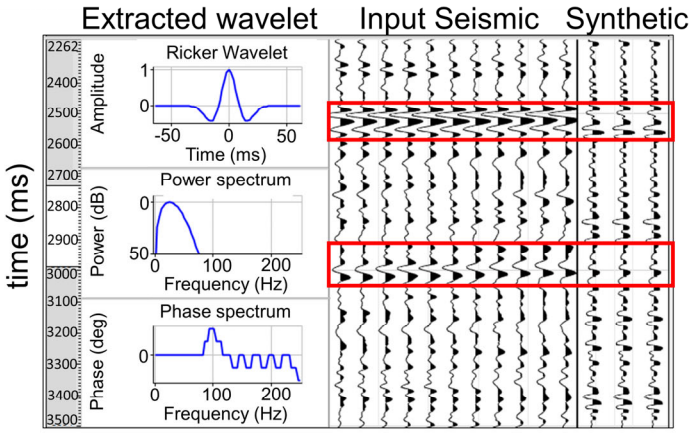

Figure 3.20: Well to seismic tie for the wavelet extraction process from L-30 well. The red boxes highlight the high similarities between the input seismic and the synthetic seismogram that is created by Petrel.

Wavelet is the crucial input in the inversion process to convert the generated pseudo-logs of V_P and ρ to synthetic seismic traces, and it should be extracted from the original seismic data. Based on the deterministic wavelet extraction method, Petrel software was used to generate the wavelet from seismic data, considering the best-match for the created synthetic seismograms for both wells. Figure 3.20 shows the correlation between the generated synthetic seismogram and the seismic data based on the sonic and density logs from well L-30. By doing the well to seismic tie procedure, and since the generated synthetic seismogram is quite similar to the original seismic data, the wavelet (50 Hz) is extracted from the seismic data.

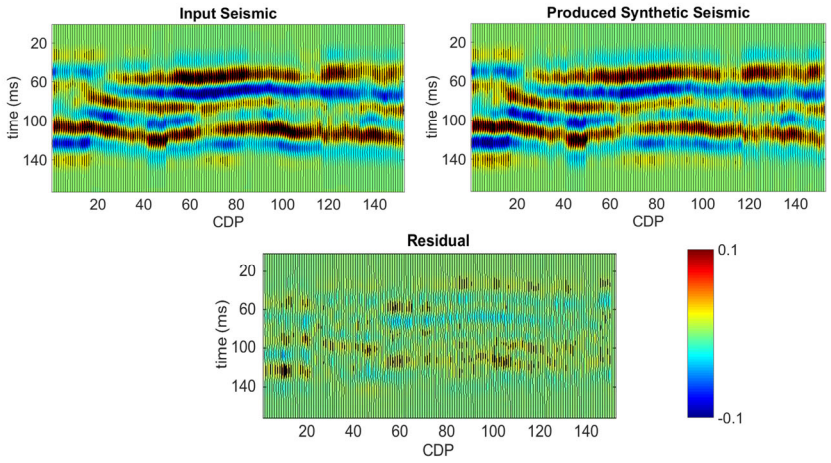

Figure 3.21: Input seismic section, produced synthetic seismic, and the difference sample-by-sample between them (residual) for all obtained solutions after eight iterations and 60 draws of the proposed inversion approach.

In the inversion, for each WAVESIM realization pseudo-well, 60 draws of V_p and ρ were sampled for all CDP locations, and the best-fit synthetic traces compared to the input seismic traces, accordingly, are retained. After eight iterations, and based on the cross-correlation cut-off (0.7), the best WAVESIM realization that produces the best-match synthetic seismogram with respect to recorded seismic data was selected. Figure 3.21 shows the generated synthetic seismogram, the input seismic section, and the corresponding residual section. The residual section indicates a high similarity between the input and synthetic seismic data.

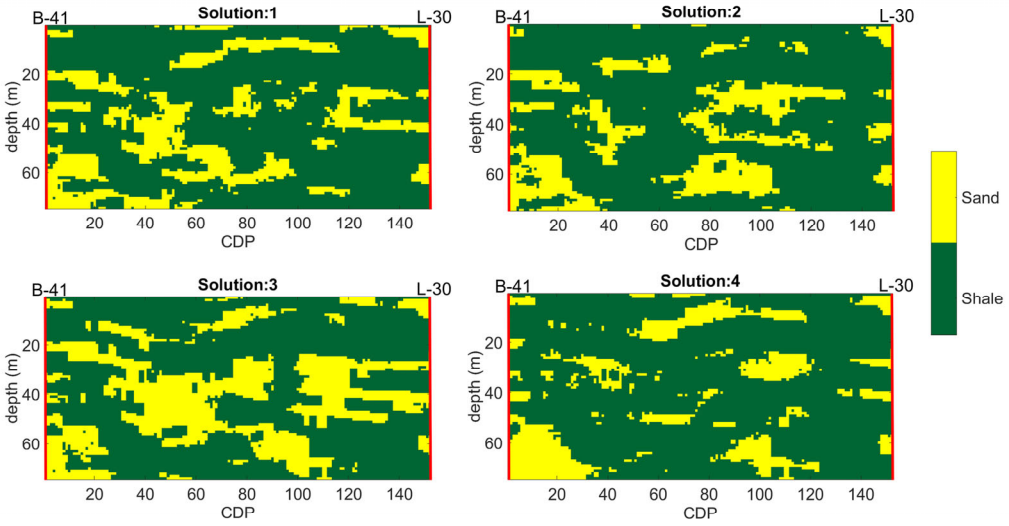

Figure 3.22: Four solutions are obtained from multiple sets of the WAVESIM realizations after eight iterations and 60 draws of the proposed inversion approach.

Stochastically, four different independent solutions (geologic scenarios) that were generated after eight iterations of the proposed inversion approach (Figure 3.22). Each of these geologic scenarios was resulted from ten WAVESIM realizations, and display various spatial arrangement of the litho-facies for the Mississauga reservoir. Figure 3.23 shows the normalized frequency or probability (E-type), and variance maps from ten lithofacies inverse solutions represent different equiprobable geologic scenarios for the study area. The shape and distribution of the major geologic bodies (sand channels) are precisely localized and observed in the normalized frequency maps. From the variance map, it can be seen that the variance values are quite low near to the wells and increases away from the wells. The shape and distribution of the major geologic bodies (sand channels) are precisely localized and observed in the probability maps. These results demonstrate the inversion approach powerful in predicting the extension of the reservoir characterization in the Penobscot field and offer an initial step to reconsider the development plans for the Mississauga reservoir.

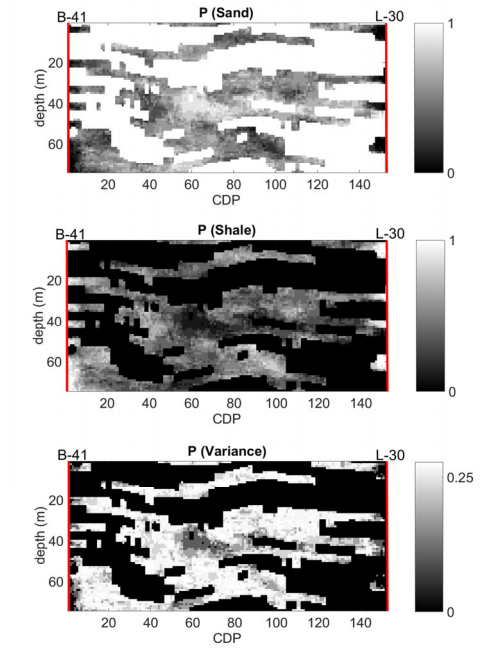

Figure 3.23: Probability or normalized frequency (E-type) and variance maps for the two assigned lithofacies groups (sand and shale), from the geological model in Figure 3.16, are estimated with multiple sets of the WAVESIM realizations constrain seismic data, which were computed after 60 draws and eight iterations of the proposed inversion approach.

Chapter 4: Conclusions and Future Work

We have developed a novel inversion approach that integrates the physical properties of litho-facies, geophysical data, and advanced multiple-point geostatistics to generate explicit stochastic solutions that precisely localized the shape and distribution of the litho-facies spatial arrangement that was observed in the conceptual geological models. A multiple-point geostatistics method, WAVESIM algorithm, provides a fast technique compared to the conventional geostatistical approaches, in generating multiple litho-faces realizations based on training image and conditioned to well positions. The Kernel density estimation technique affords an appropriate method in estimating the likelihoods of the elastic properties (V_P and ρ) and a proper discriminating tool to detect the suitable well that subsequently used for the drawing process in the inversion approach. From the probability maps (E-type), the generated WAVESIM realizations can correctly detect the geologic bodies (i.e., channels) in the well positions of the training image; however, without constraining geophysical data, the shape and distribution of channels cannot be identified. The results of either synthetic or the Penobscot dataset validate our inversion approach and show the strong applicability of this technique in predicting the extension of the reservoir characterization in the Penobscot field and offer an initial step to reconsider the development plans for the Mississauga reservoir. The probability or normalized frequency maps (E-type) provide a powerful visualization tool for the inversion solutions that probability values away from the well locations are significantly improved as compared to the probability maps from WAVESIM without constraining to geophysical data. It was also observed from variance maps of the inversion solutions that variance values are very low near to the wells and increases away from the wells.

This research presented the proposed inversion loop encountered two elastic properties (Vp and ρ); however, the proposed algorithm is not limited to acoustic impedance. The elastic reflectivities can be estimated inside the inversion loop, and then convolved with the given wavelet to produce the appropriate synthetic seismograms. The inversion loop is designed to generate a synthetic seismogram in the time domain by utilizing multiple numbers of

iterations. As a consequence, this procedure can take a long time of running due to several repetitions. The computational time can significantly be improved by generating synthetic seismograms in the frequency domain.

5 Reference List

Arpat, B. G., 2005, Sequential simulation with patterns: Ph.D. dissertation, Stanford University.

Arpat, G. B., & Caers, J. (2005). A multiple-scale, pattern-based approach to sequential simulation. In Geostatistics Banff 2004 (pp. 255-264). Springer, Dordrecht.

Arpat, G. B., & Caers, J. (2007). Conditional simulation with patterns. Mathematical Geology, 39(2), 177-203.

Azizian, M., & Davis, T. L. (2018). Stochastic inversion of seismic data by implementing image-quilting to build a lithofacies model for reservoir characterization of Delhi Field, Louisiana. First Break, 36(9), 47-57.

Azevedo, L., Nunes, R., Correia, P., Soares, A., Guerreiro, L., & Neto, G. S. (2014). Multidimensional scaling for the evaluation of a geostatistical seismic elastic inversion methodology. Geophysics, 79(1), M1-M10.

Azevedo, L., Nunes, R., Soares, A., Mundin, E. C., & Neto, G. S. (2015). Integration of well data into geostatistical seismic amplitude variation with angle inversion for facies estimation. Geophysics, 80(6), M113-M128.

Boisvert, J. B., Pyrcz, M. J., & Deutsch, C. V. (2007). Multiple-point statistics for training image selection. Natural Resources Research, 16(4), 313-321.

Bortoli, L. J., Alabert, F., Haas, A., & Journel, A. (1993). Constraining stochastic images to seismic data. In Geostatistics Tróia'92 (pp. 325-337). Springer, Dordrecht.

Bosch, M., Mukerji, T., & Gonzalez, E. F. (2010). Seismic inversion for reservoir properties combining statistical rock physics and geostatistics: A review. Geophysics, 75(5), 75A165-75A176.

Buland, A., & Omre, H. (2003). Bayesian linearized AVO inversion. Geophysics, 68(1), 185-198.

Bo, Y. Y., Lee, G. H., Kim, H. J., Jou, H. T., Yoo, D. G., Ryu, B. J., & Lee, K. (2013). Comparison of wavelet estimation methods. Geosciences Journal, 17(1), 55-63.

Caers, J., Strebelle, S., & Payrazyan, K. (2003). Stochastic integration of seismic data and geologic scenarios: A West Africa submarine channel saga. The Leading Edge, 22(3), 192-196.

Campbell, T. J., Richards, F. B., Silva, R. L., Wach, G., & Eliuk, L. (2015). Interpretation of the Penobscot 3D seismic volume using constrained sparse spike inversion, Sable sub-Basin, offshore Nova Scotia. Marine and Petroleum Geology, 68, 73-93.

Castro, S., Caers, J., & Mukerji, T. (2005). The Stanford VI reservoir 18th Annual Report Stanford Center for Reservoir Forecasting (California: Stanford University).

Chatterjee, S., Dimitrakopoulos, R., & Mustapha, H. (2012). Dimensional reduction of pattern-based simulation using wavelet analysis. Mathematical Geosciences, 44(3), 343-374.

Chatterjee, S., & Dimitrakopoulos, R. (2012). Multi-scale stochastic simulation with a wavelet-based approach. Computers & geosciences, 45, 177-189.

Chatterjee, S., & Mohanty, M. M. (2015). Automatic cluster selection using gap statistics for pattern-based multi-point geostatistical simulation. Arabian Journal of Geosciences, 8(9), 7691-7704.

Chatterjee, S., Mustapha, H., & Dimitrakopoulos, R. (2016). Fast wavelet-based stochastic simulation using training images. Computational Geosciences, 20(3), 399-420.

Connolly, P. A., & Hughes, M. J. (2016). Stochastic inversion by matching to large numbers of pseudo-wells. Geophysics, 81(2), M7-M22.

Gloaguen, E., & Dimitrakopoulos, R. (2009). Two-dimensional conditional simulations based on the wavelet decomposition of training images. Mathematical Geosciences, 41(6), 679-701.

González, E. F. (2006). Physical and quantitative interpretation of seismic attributes for rocks and fluids identification. Stanford University.

González, E. F., Mukerji, T., & Mavko, G. (2007). Seismic inversion combining rock physics and multiple-point geostatistics. Geophysics, 73(1), R11-R21.

Grana, D., & Della Rossa, E. (2010). Probabilistic petrophysical-properties estimation integrating statistical rock physics with seismic inversion. Geophysics, 75(3), O21-O37.

Grana, D., Mukerji, T., Dvorkin, J., & Mavko, G. (2012). Stochastic inversion of facies from seismic data based on sequential simulations and probability perturbation method. *Geophysics*, *77*(4), M53-M72.

Guardiano, F. B., & Srivastava, R. M. (1993). Multivariate geostatistics: beyond bivariate moments. In Geostatistics Troia'92 (pp. 133-144). Springer, Dordrecht.

Haas, A., & Dubrule, O. (1994). Geostatistical inversion-a sequential method of stochastic reservoir modelling constrained by seismic data. *First break*, *12*(11), 561-569.

Journel, A. G., & Ying, Z. (2001). The theoretical links between sequential Gaussian simulation, Gaussian truncated simulation, and probability field simulation. Mathematical Geology, 33(1), 31-40.

Kendell, K., Brown, D. E., & Smith, B. M. (2014). Geological context and parcel prospectivity for Call for Bids NS13-1; seismic Interpretation, source rocks and maturation, exploration history and potential play types of the central and eastern Scotian Shelf., Canada–Nova Scotia Offshore Petroleum Board, Geoscience Open File Report.

Liu, X., Li, J., Chen, X., Guo, K., Li, C., Zhou, L., & Cheng, J. (2018). Stochastic inversion of facies and reservoir properties based on multi-point geostatistics. Journal of Geophysics and Engineering, 15(6), 2455-2468.

Mariethoz, G., Renard, P., & Straubhaar, J. (2010). The direct sampling method to perform multiple-point geostatistical simulations. Water Resources Research, 46(11).

Mariethoz, G., & Caers, J. (2014). Multiple-point geostatistics: stochastic modeling with training images. John Wiley & Sons.

Mustapha, H., Chatterjee, S., Dimitrakopoulos, R., & Graf, T. (2013). Geologic heterogeneity recognition using discrete wavelet transformation for subsurface flow solute transport simulations. Advances in water resources, 54, 22-37.

Ruggeri, P., Irving, J., Gloaguen, E., & Holliger, K. (2013). Regional–scale integration of multiresolution hydrological and geophysical data using a two-step Bayesian sequential simulation approach. Geophysical Journal International, 194(1), 289-303.

Russell, B. H. (1988). Introduction to seismic inversion methods (No. 2). SEG Books.

Scales, J. A., & Tenorio, L. (2001). Prior information and uncertainty in inverse problems. Geophysics, 66(2), 389-397.

Strebelle, S. B. (2002). Sequential simulation drawing structures from training images.

Strebelle, S. (2002). Conditional simulation of complex geological structures using multiple-point statistics. Mathematical geology, 34(1), 1-21.

Tahmasebi, P. (2018). Multiple point statistics: a review. In Handbook of Mathematical Geosciences (pp. 613-643). Springer, Cham.

Tarantola, A. (2005). Inverse problem theory and methods for model parameter estimation (Vol. 89).

Tran, T. T. (1994). Improving variogram reproduction on dense simulation grids. Computers & Geosciences, 20(7-8), 1161-1168.

https://wiki.seg.org/wiki/Open_data